INDIAN JOURNAL OF SCIENCE AND TECHNOLOGY

RESEARCH ARTICLE

Deep Learning based Mobilenet with Deep Belief Network for Lung Cancer Diagnosis in IOT and Cloud Enabled Environment

I Jasmine Selvakumari Jeya[1]*, Dinesh Valluru[2], A Sherin[3]

1 Professor, Department of Information Technology, Hindusthan College of Engineering and Technology, Coimbatore, 641032, Tamil Nadu, India
2 Associate Professor, Department of Computer Science and Engineering, SRK Institute of Technology, Vijayawada, 521 108, Andhra Pradesh, India
3 Assistant Professor, Department of Computer Science and Engineering, Hindusthan College of Engineering and Technology, Coimbatore, 641 032, Tamil Nadu, India

OPEN ACCESS

Received: 10-07-2022
Accepted: 01-09-2022
Published: 10-11-2022

Citation: Jeya IJS, Valluru D, Sherin A (2022) Deep Learning based Mobilenet with Deep Belief Network for Lung Cancer Diagnosis in IOT and Cloud Enabled Environment. Indian Journal of Science and Technology 15(42): 2219-2229. https://doi.org/10.17485/IJST/v15i42.1435

* **Corresponding author**.

wjasminejeya@gmail.com

Funding: None

Competing Interests: None

Published By Indian Society for Education and Environment (iSee)

ISSN
Print: 0974-6846
Electronic: 0974-5645

Abstract

Background: The purpose of the present investigation is to unravel the complexity involved in Lung Cancer diagnosis by inculcating a new automated deep learning based MobileNet (DLMN) with deep belief network (DBN), called DLMN-DBN model in Internet of Things and cloud enabled environment. **Methods**: This paper presents an optimal DLMN-DBN model for lung cancer diagnosis where the parameters of DLMN-DBN model are optimized, and feature extraction and classification takes place by DLMN and DBN model respectively. The experimentation part takes place on four dimensions: 1) IoT devices enabled data acquisition for lung cancer diagnosis and the data are transmitted to the cloud server for diagnostic process, 2) the Guassian Filtering (GF) based preprocessing technique for noise removal, 3) feature extraction using DLMN model and 4) Optimal classification using DBN model. For experimental validation, an extensive experimentation analysis is performed to highlight the superior diagnostic outcome of the DLMN-DBN model. **Findings**: The experimental values stated that the DLMN-DBN model has resulted in superior results when compared with existing models with higher accuracy, sensitivity, and specificity of 95.55%, 93.94%, and 96.49% respectively. **Novelty and applications**: The new state of the art DLMN-DBN model and its robustness help general practitioners efficiently and effectively diagnose lung cancer conditions at the initial stage thereby reducing further complications and morbidity.

Keywords: Lung cancer; Diagnosis; Classification; Deep learning; MobileNet; Deep belief network

1 Introduction

In recent times, the rapid development of Internet of Things (IoT) and cloud computing (CC) environment takes healthcare services to the next level[1,2]. The e-healthcare services are commonly available using IoT devices to generate data and utilized cloud technologies to store, process, and access it. On the other hand, lung cancer is recognized as a risky illness that raises the global mortality rate yearly. Medical imaging plays a vital role in the healthcare domain involving non-invasive medication and clinical investigation. Collected restorative images namely X-ray, computed tomography (CT), and ultrasound imaging techniques are commonly employed to diagnose diseases. On medicinal imaging, CT scan is one of the effective tools widely used for capturing images in films. Lung cancer is a type of cancer which results in a mortality rate of 1.61 million deaths annually. Global, an estimated 19.3 million new cancer cases and almost 10.0 million cancer deaths reported in 2020.[3,4]. The survival rate gets improved when cancer gets detected at earlier levels. Earlier identification of lung cancer is a tedious process. Approximately 80% of the patients are detected proficiently only at the later stages of cancer[5]. The detection of lung cancer has different stages of operations namely preprocessing, segmentation, feature extraction, and classification. Image preprocessing is commonly applied to remove the noise that exists in the CT image. Then, feature extraction takes place to filter out the set of feature vectors from the CT images. An important characteristic of CT images is the nature of non-obtrusiveness. The chosen or filtered features extracts the compared details from the input data to the reduction system. The reduced features are allocated to a classifier which is commonly employed for training and testing processes.

Several research works are carried out for lung cancer detection from CT images using artificial intelligence, and machine learning (ML) models[6]. But they are costly and can detect cancer only at the later stages resulting in low survival rate. Earlier identification of cancer with the help of to cure the disease totally. Therefore, there is a requirement to identify the presence of cancer cells in the primary stage.

In 2019, Shakeel et al. introduced an automatic Lung cancer detection method based on CT scan images[7]. They employed bin smoothing normalization for image de-noising and selected features using the minimum repetition and Wolf heuristic feature selection process. The utmost fascinating method of this study is the classifier's excellency; they used a Discrete AdaBoost optimized ensemble learning generalized neural network (DAELGNN) for classification accuracy. Toraman et al. presented a study whose goal was to classify colon cancer's likelihood using Fourier Transform Infrared (FTIR) spectroscopy signals[8]. In their proposed work, they extracted several statistical features from those signals and then used SVM and ANN to classify them, which resulted in excellent classification accuracy (ANN).

In 2020, Suresh and Mohan presented a lung cancer diagnosis method based on nodule region of interest (ROI)-based feature learning using CNN. In the proposed work they collected CT scan images from the Lung Image Database Consortium (LIDC) and Infectious Disease Research Institute (IDRI) databases and used Generative Adversarial Networks (GANs) to produce additional images to increase the sample size. They attained a 93.9% classification accuracy using CNN-based classification algorithms[9,10]. Masud et al. presented a pulmonary nodule detection method based on CT scan images using a light CNN architecture[11]. Verified on the LIDC dataset, their model accomplished excellent classification accuracy while distinguishing among normal, benign, and malignant cases. Shakeel et al. introduced another CT scan image-based lung cancer detection method. Upon removing noise from the images, they used an Improved Deep Neural Network (IDNN) for image segmentation and various Ensemble Methods (EM) for image classification[12].

Different works are projected for developing the automated lung cancer diagnosis model for the identification of lung cancer. This paper presents an effective lung cancer diagnosis in IoT and cloud enabled environment using deep learning based MobileNet (DLMN) with deep belief network (DBN), called DLMN-DBN model. The presented DLMN-DBN model involves preprocessing, feature extraction, and classification. The presented DLMN-DBN model executes the Gaussian filtering (GF) based preprocessing for removing the noise that exists in the lung CT images. Followed by, DLMN model-based feature extractor is utilized to extract a useful set of feature vectors. Besides, DBN based classification model is applied to determine the appropriate class labels of lung cancer. A series of simulations were performed to ensure the effective results analysis of the DLMN-DBN model. And this generic model presented in this paper demonstrates excellent diagnostic measure for the lung cancer at the initial stage with minimal cost and at the earlier stage thereby reduces further complications in the future.

2 Methodology

2.1 The Proposed DLMN-DBN model

Figure. 1 showcases the working process of the DLMN-DBN model. The figure states that the input lung CT images are initially collected using internet of things (IoT) devices attached to the human body and is transferred to the cloud server for further computation. At that point, they are preprocessed using GF technique for removing the noise that exists in it. Then, the feature

vectors are extracted using DLMN model and finally, classification process takes place by the use of DBN model.

2.2 GF based Preprocessing

Here, pre-processing of lung CT images takes place in two levels namely Guassian Filtering (GF) based noise eliminate and Contrast Limited Adaptive Histogram Equalization (CLAHE) based contrast enhancement[13]. The main advantage of the GF is that its Fourier transform is also a Gaussian distribution centered around the zero frequency. On the other hand, the main advantage of CLAHE is that it will result in higher quality output images. Doing so benefits doctors and radiologists better interpret the scans and make a precise diagnosis.

By the use of 2D GF technique, the noise removal and smoothening processes are carried out on CT lung images. The convolutional operator is defined to be the Gaussian function and the policy of Gaussian smoothing is obtained by the use of convolution.

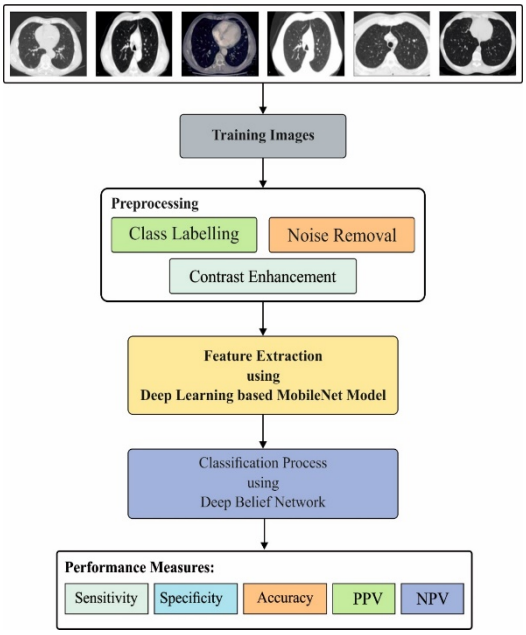

Fig 1. Working process of DLMN-DBN model

So, the Gaussian operator in 1D can be represented as follows:

$$G_{1D}(x) = \frac{1}{\sqrt{2\pi}\sigma} e^{-\left(\frac{x^2}{2\sigma^2}\right)}. \tag{1}$$

A notable smoothing image filtering technique undergo localization in the spatial and frequency domains; henceforth, the uncertainty relationship can be fulfilled using Eq. (2):

$$\Delta x \Delta \omega \geq \frac{1}{2}. \tag{2}$$

The Gaussian operator in $2D$ can be defined as follows:

$$G_{2D}(x,y) = \frac{1}{2\pi\sigma^2} e^{-\left(\frac{x^2+y^2}{2\sigma^2}\right)}, \tag{3}$$

where σ defines the Standard Deviation (SD) of Gaussian function. If the values are high, then the smoothening process will be high. In addition, $(x,\ y)$ denotes the Cartesian coordinate points of the image representing the window dimensions. The GF

comprises the addition and multiplication operations carried out on the images and the kernel of the image can be defined in a matrix format in the range of 0-255. Therefore, the kernel is normalized into a square matrix in the range of 0-1. Followed by a kernel can be represented using a bit count. In case of a convolutional model, the individual bits of the kernel are multiplied with the element of the image which is divided by the power of 2. The convolutions can be represented as the multiplication task and the offered logarithm multiplication is ineffective in terms of accuracy. So, an effective remarkable logarithm multiplication model is needed for GF to determine the real-time performance and is employed to attain better outcome.

2.2.1 CLAHE based Contrast Enhancement

When the noise filtration process takes place using GF technique, CLAHE model is employed to improve the contrast of the CT lung images. In addition, the intensities of the pixels transform a value in a particular range which is related to the pixel intensity's grade in local intensity histogram. Besides, CLAHE is developed based on Adaptive Histogram Equalization (AHE) where the images are enhanced using a user-based clip level, indicating the height of a local histogram. Here, the enhancement process takes place on minimum patch. Generally, the CLAHE technique is commonly employed for limiting the shadows of the edge and noise produced in the homogenous regions of the clinical images. This technique is used to improvise the CT images and offered effective outcome. The input image I with the size of $M \times N$, can be categorized into smaller blocks. Furthermore, CLAHE is employed to improvise the contrast level of all individual blocks. As a result, the bilinear interpolation is employed to unify the nearby blocks and transforms them into an entire image. Few processes that exist in the CLAHE technique are listed as follows.

1) The patches of the image are divided into a set of non-overlapping blocks with the size 8×8.
2) For every block, the histogram is determined.
3) For determining the contrast enhancement, a clip boundary of histogram, $t = 0.001$, is assigned.
4) When the clipping of threshold values takes place, then the redistribution of histogram is performed.
5) The expansion of histogram blocks take place by the use of transformation function:

$$A_t = \sum_{i=0}^{t} p_t\left(A_i\right), \tag{4}$$

where $p_t(A_i)$ defines a probability density function of the patch of the grayscale image value at i and is defined by:

$$p_t(A_i) = \frac{m_i}{m}, \tag{5}$$

where m_i represents a grayscale value of the input pixel i and m denotes the number of pixels in the block.

6) Bilinear interpolation is applied to combine the nearby blocks in every patch. Therefore, the grayscale value of the patch is altered depending upon the new histogram.

Here, a block of size 8×8 and clip limit of histogram as 0.001 are applied.

2.3 DLMN based Feature Extraction

Generally, DL is a popular method which is developed from the multi-layer feed forward neural networks (FFNN)[14]. By the design of high-end systems, it is feasible to train deep networks using multi-level NN. The CNN operates effectively in several research areas like object detection, speech recognition, etc. The CNN is inspired by the multi-layer NN. Fascinatingly, the main benefit of CNN architecture is the extraction of features that assist in reducing the pre-processing stage to a certain level. Therefore, it is non-essential to carry out a pre-examination to identify the features that exist in the image. The CNN comprises input, convolution, pooling, Fully Connected (FC), rectified linear unit (ReLU), Dropout as well as classifier layers. The exclusive outcome of every layer can be represented as follows.

• **Input layer:** It is employed to design the initial layer of CNN where the data is given into the model without any processing. In addition, the input data size varies between one another where the pretraining DL models are used.

• **Convolution layer**: It is the second layer that exists in CNN that is utilized to extract features through the pixel matrix of the images. It is based on the circulation of a particular filter over the entire image and it results in an effective image matrix.

• **ReLU layer**: It is inserted next to the convolution layer. It is assumed as the activation function which takes the negative values as input and led to 0. An important use is the differentiation of the functions from the activation function such as hyperbolic tangent, sinus that has the ability to produce proficient outcome. Generally, they are used for the non-linear transformation process.

• **Pooling layer:** It is performed next to convolution and ReLU functions. A major premise of the layer is given for limiting the size of the input and discard the system from recording. For convolutional layer, pooling function employs distinct filter

sizes. They make use of average pooling function on the image matrix with particular step variable. At this point, maximum pooling is recommended.

• **Fully connected layer**: It comes next to the Convolution, ReLU, and Pooling layers. The neurons that exist in this layer are totally linked to other regions of the previous layers.

• **Dropout layer:** It is employed of removing the memory of the network. The outcome of the model is based on the arbitrary deletion of particular set of nodes in the network.

• **Classifier layer**: It is produced next to FC Layer where classification process is performed. During the classification task, the possible values are applied to exhibit whether they are located closer to the class. These probability values are achieved using the softmax function.

The MobileNet model is devised for enhancing the real word outcome of the DL model with restricted hardware units[15,16]. It could minimize the parameter count with no sacrifice in accuracy. Earlier works have displayed that the MobileNet requires 1/33 of the variables of Visual geometry group-16 (VGG-16) for achieving the identical classifier outcome on the ImageNet classification process. The structure of MobileNet is given in Figure 2. The *Conv_Dw_Pw* is a deeper and separate convolution structure. It involves depthwise (Dw) and pointwise (Pw) layers. The Dw are deep convolutional layers which comprise a set of 3×3 kernels, whereas the Pw are mutual convolutional layer uses 1×1 kernels. The convolutions outcome is considered using the batch normalization (BN) technique and activation function ReLU.

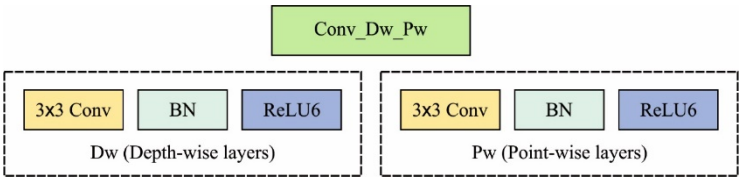

Fig 2. Structure of MobileNet

Here, the ReLU activation function is substituted by *ReLU*6, and the BN process is performed, supporting the automated alteration of data distribution. The ReLU6 activation function is defined in Eq. (6)

$$y = \ min\left(max\left(z, 0\right), 6\right) \tag{6}$$

where z is the value of all the pixels that exist in the feature map. In addition, the deep and separable convolution model allows the MobileNet for increasing the training process and considerably decreases the computation complexity due to the following facts. The general convolution can be defined by

:

$$G_N = \sum_M^{K_{M,N} * F_M} \tag{7}$$

where $K_{M,N}$ is the filter; and M and N indicate the input and output channel count corresponding. At the time of general convolution process, the input images comprising the feature image, F_M denotes the input image, with feature map make use of zero paddings. If the sizes and input image channels are represented as $D_F * D_F$ and M, it is essential to hold N filters with M channels and the $D_K * D_K$ size prior to outcome, and N feature images with the size of $D_K * D_K$. The computation cost can be defined by $D_K * D_K * M * N * D_F * D_F$. Contrastingly, the Dw formula can be defined by

$$\widehat{G}_M = \sum \widehat{K}_{1,M} * FM \tag{8}$$

where $\widehat{K}_{1,M}$ is the filter. F_M holds the identical meaning as given in Eq. (7). In case of step size one, the zero filling ensured that the feature map size is not variable next to the utilization of deep and separable convolutional structure. Figure 3 demonstrates the layered of MobileNet.

If the step size is two, the zero-filling ensured that the feature map size becomes half of the feature map next to the utilization of deep and separable convolutional structure and thereby dimensional reduction process is implemented. The deep separable convolutional network of MobileNet obtains the identical output of the classical convolution depending upon the identical input. The Dw phase desires M filters with 1 channel and the size of $D_K * D_K$. The Pw stage requires N filters with M channels and the size of 1×1. Here, the computational cost of the deep separable convolutional structure is $D_K * D_K * M * D_F * D_F + M * N * D_F * D_F$, about $\frac{1}{N} + \frac{1}{D_K^2}$ of that of typical convolution. Also, the data distribution would be

Type / Stride	Filter Shape	Input Size
Conv / s2	3 x 3 x 3 x 32	224 x 224 x 3
Conv dw / s1	3 x 3 x 32 dw	112 x 112 x 32
Conv / s1	1 x 1 x 32 x 64	112 x 112 x 32
Conv dw / s2	3 x 3 x 64 dw	112 x 112 x 64
Conv / s1	1 x 1 x 64 x 128	56 x 56 x 64
Conv dw / s1	3 x 3 x 128 dw	56 x 56 x 128
Conv / s1	1 x 1 x 128 x 128	56 x 56 x 128
Conv dw / s2	3 x 3 x 128 dw	56 x 56 x 128
Conv / s1	1 x 1 x 128 x 256	28 x 28 x 128
Conv dw / s2	3 x 3 x 256 dw	28 x 28 x 256
Conv / s1	1 x 1 x 256 x 256	28 x 28 x 256
Conv dw / s1	3 x 3 x 256 dw	28 x 28 x 256
Conv / s1	1 x 1 x 256 x 512	14 x 14 x 256
5 x Conv dw / s1	3 x 3 x 512 dw	14 x 14 x 512
5 x Conv / s1	1 x 1 x 512 x 512	14 x 14 x 512
Conv dw / s2	3 x 3 x 512 dw	14 x 14 x 512
Conv / s1	1 x 1 x 512 x 1024	7 x 7 x 512
Conv dw / s2	3 x 3 x 1024 dw	7 x 7 x 1024
Conv / s1	1 x 1 x 1024 x 1024	7 x 7 x 1024
Avg Pool / s1	Pool 7 x 7	7 x 7 x 1024
FC / s1	1024 x 7	1 x 1 x 1024
GNB, SVM / s1	Classifier	1 x 1 x 7

Fig 3. Layered of MobileNet

altered by every convolutional layer at the time of training the network. When the data is on the edges of the activation function, the gradients get disappeared and the parameters are not updated. Next to the typical normal distribution, the BN technique modifies the data by fixing 2 learning variables such as learning rate and dropout ratio to prevent the gradient vanishing problem.

2.4 DBN based Classification

Finally, the extracted feature vectors are fed into the DBN model for the classification of lung CT images. The architecture of the DBN model is depicted in Figure 4.

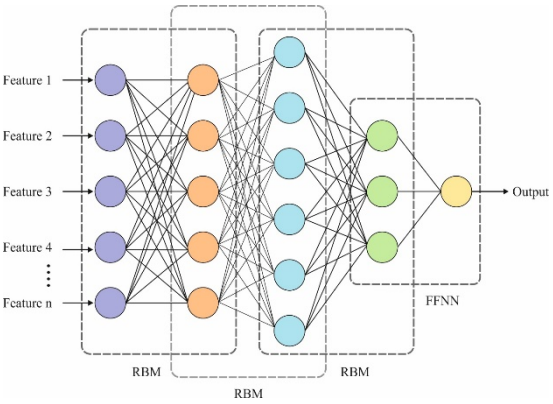

Fig 4. Structure of DBN

It comprises a stacked restricted Boltzmann machines (RBMs) and a classification model in the deep network. The training process of DBN comprises unsupervised and supervised learning phase. The stacked RBM regions are placed in the classifier layer for the generation of the DBN model. The DBN training process begins with the unsupervised training of RBM by the use of greedy technique and outcome of the earlier RBM becomes the input of the subsequent RBM. At last, the supervised training process is carried out in the classifier layer of the DBN model. Generally, a major variation among the DBN and Multi-Layer Perceptron (MLP) is that the DBN has the ability to carry out the learning process via layer-by-layer unsupervised training

process. But the MLP failed to execute feature learning tasks and is commonly employed for classification. The resemblance between the DBN and MLP is that they are FC network and utilized BP technique for supervised learning. is performed in the classification layer of DBN. The RBM is a probability based graphical network comprehended by the stochastic NN where only two outputs state of the neurons is involved. It is based on the Boltzmann machine (BM) and is a feature extraction technique depending upon the energy model and optimization takes place via unsupervised training. The RBM model comprises a two set of layers namely visible layer $v = (v_1, v_2 \ldots, v_n)$ indicating the observational data, and hidden layer $h = (h_1, h_2 \ldots, h_m)$ which can be defined as the feature extraction layer. Principally, the uppermost two layers are represented as the joint distribution of the latter hidden layer (h_l) and the output layer, also known as the associative memory element.

The learning procedure of the DBN model undergoes partition into two stages such as unsupervised learning (pretraining) and supervised learning (fine-tuning). Initially, the unsupervised learning is realized through contrastive divergence for training the stack of RBMs in a hierarchical way. Next, the supervised learning is instigated by the BP technique for fine-tuning the initial weights and biases of the entire network[17,18]. A major intention of unsupervised training in DBN is the optimization of RBMs for extracting the features from the data. For a provided set of (v, h), the energy function $E(v, h|\theta)$ is defined as follows:

$$E(v, h|\theta) = -\sum_{i=1}^{n} a_i v_i - \sum_{j=1}^{m} b_j h_j - \sum_{i=1}^{n} \sum_{j=1}^{m} v_i w_{ij} h_j \tag{9}$$

where $\theta = (W_{ij}, a_i, b_j\}$ is the variable in RBM, where w indicates the weights of the layer connections, and a and b are the biases of the visible and the hidden layer neurons, correspondingly. The joint probability distribution can be defined by:

$$P(v, h|\theta) = \frac{e^{-E(v,h|\theta)}}{Z(\theta)}, \; Z(\theta) = \sum_{v,h} e^{-E(v,h|\theta)} \tag{10}$$

At the time of Gibbs sampling process, the condition probability distribution of the visible and hidden neurons is indicated as

$$P(h_j = 1|v, \theta) = sigmoid\left(b_j + \sum_i^{v_i w_{ij}}\right) \tag{11}$$

$$P(v_i = 1|h, \theta) = sigmoid\left(a_i + \sum_j^{h_j w_{ji}}\right) \tag{12}$$

Using Eq. (11), the probability that h_j is an active state which can be defined. As RBM has a symmetric feature for the defined hidden layer state h, the activation state probability of all the neurons in the visible layer is equated in Eq. (12). These processes are applied for obtaining the respective weight w of RBM, and the unsupervised learning of DBN trains the RBM in a hierarchical way for obtaining the entire initial weight $W = (w_1, w_2 \ldots w_l\}$. Supervised learning involves fine-tuning the connection weights generated from the unsupervised learning. The BP technique will determine the gradients by labeling the training dataset and modifies the network parameters among the layers for reducing the gradients. At last, the deep network structure with least predictive error is designed.

3 Results and Discussions

3.1 Performance Validation

The performance of the DLMN-DBN model has been validated using the lung database and the details are given in Table 1. The dataset holds a total of 100 images with three class labels, namely benign, malignant, and normal. Few sample test images are showcased in Figure 5(a)

Figure 5 (b) and (c) visualizes the results of the sample test image with the preprocessed image.Figure 5a shows the actual image and its preprocessed version is depicted in Figure 5b.

Similiarly, Figure 6 displays the visualization outcomes of the sample input images with the classified outcomes. Figure 6a showcases the preprocessed images and the classified images are demonstrated in Figure 6b.

Table 2 displays the confusion matrix generated by the DLMN-DBN model on the classification of lung images. In addition, the values in Table 2 are manipulated in terms of TP, TN, FP, and FN in Table 3. On the applied training phase, the DLMN-DBN model has proficiently classified 26, 20, and 19 images under Normal, Malignant, and Benign classes respectively.

Besides, on the applied testing phase, the DLMN-DBN model has competently classified 8, 10, and 10 images under Normal, Malignant, and Benign classes respectively.

Table 4 provides the results analysis of the DLMN-DBN model in terms of distinct measures on the applied training and testing phases. The DLMN-DBN model has identified the Normal class images with a sensitivity (sens.0 of 96.30%, specificity

Table 1. Dataset Description

Description	Lung Database
Number of Classes	3
Classes (Normal /Malignant/ Benign)	Labels (0/1/2)
Number of Images in Benign	32
Number of Images in Malignant	33
Number of Images in Normal	35
Total Number of Images	100
Data source	[30,31]

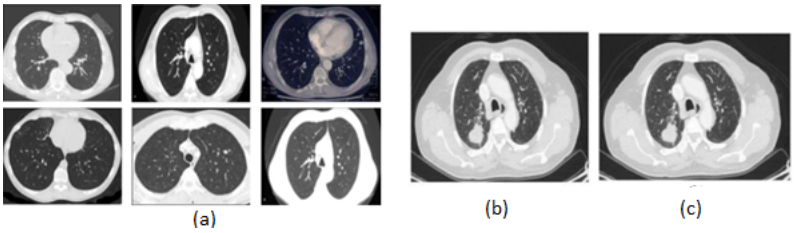

Fig 5. (a) Sample Images (b) Original Image (c) Preprocessed Image

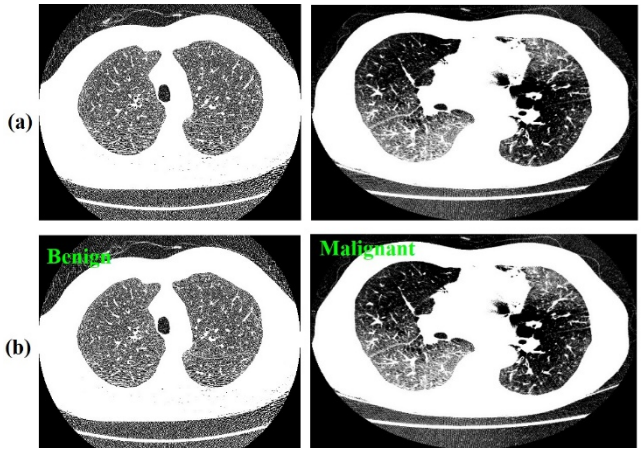

Fig 6. (a) Preprocessed Image (b) Classified Image

Table 2. Confusion Matrix of Proposed Method on Applied Dataset

Input Label	Training Phase			Total No. of Images
	Normal	Malignant	Benign	
Normal	26	0	1	27
Malignant	1	20	1	22
Benign	0	2	19	21
Total No. of Images	27	22	21	70
Input Label	**Testing Phase**			**Total No. of Images**
	Normal	**Malignant**	**Benign**	
Normal	8	0	0	8
Malignant	0	10	1	11
Benign	0	1	10	11
Total No. of Images	8	11	11	30

Table 3. Manipulations from Confusion Matrix

Classes	Training Phase			Testing Phase		
	Normal	Malignant	Benign	Normal	Malignant	Benign
TP	26	20	19	8	10	10
TN	42	46	47	22	18	18
FP	1	2	2	0	1	1
FN	1	2	2	0	1	1

(spec.) of 97.97%, accuracy (acc.) of 97.14%, Positive predictive value (PPV) of 96.30%, and Negative predictive value (NPV) of 97.67%. In addition, the DLMN-DBN method has recognized the Malignant class images with the sens. of 90.91%, spec. of 95.83%, acc. of 94.29%, PPV of 90.91%, and NPV of 95.83%. Followed by, the DLMN-DBN technique has recognized the Benign class images with the sens. of 90.48%, spec. of 95.92%, acc. of 94.29%, PPV of 90.48%, and NPV of 95.92%. At the same time, the DLMN-DBN algorithm has identified the Average class images with the sens. of 90.48%, spec. of 95.92%, acc. of 94.29%, PPV of 90.48%, and NPV of 95.92%.

Table 4. Performance Measures of Training and Test Images with Different Classes on Applied Dataset

Classes	Training Phase				
	Sens.	Spec.	Acc.	PPV	NPV
Normal	96.30	97.67	97.14	96.30	97.67
Malignant	90.91	95.83	94.29	90.91	95.83
Benign	90.48	95.92	94.29	90.48	95.92
Average	90.48	95.92	94.29	90.48	95.92
Classes	**Testing Phase**				
	Sens.	**Spec.**	**Acc.**	**PPV**	**NPV**
Normal	100.00	100.00	100.00	100.00	100.00
Malignant	90.91	94.74	93.33	90.91	94.74
Benign	90.91	94.74	93.33	90.91	94.74
Average	93.94	96.49	95.55	93.94	96.49

The DLMN-DBN technique has recognized the Normal class images with the sens. of 100%, spec. of 100%, acc. of 100%, PPV of 100%, and NPV of 100%. Additionally, the DLMN-DBN approach has identified the Malignant class images with the sens. of 90.91%, spec. of 94.74%, acc. of 93.33%, PPV of 90.91%, and NPV of 94.74%. Concurrently, the DLMN-DBN method has identified the Benign class images with the sens. of 90.91%, spec. of 94.74, acc. of 93.33%, PPV of 90.91%, and NPV of 94.74%. Eventually, the DLMN-DBN methodology has recognized the Average class images with the sens. of 93.94%, spec. of 96.49%, acc. of 95.55%, PPV of 93.94%, and NPV of 96.49%.

3.2 Comparison with existing systems

An extensive comparative study is performed by taking into account of various existing approaches. The Table 5 provides a detailed comparative study of the DLMN-DBN model with existing state of art methods. The table exhibited that the linear method has accomplished inferior results by attaining a minimum acc. of 77%, sens. of 89%, and spec. of 36%. Likewise, the MLP technique has reached a somewhat higher acc. of 82%, sens. of 77%, and spec. of 72%. Followed by the RBF method has resulted in an even superior acc. of 84%, sens. of 86%, and spec. of 54%. Simultaneously, the ANN algorithm has portrayed a moderate result with an acc. of 86%, sens. of 87%, and spec. of 79%. Additionally, the DNN approach has tried to depict reasonable performance with an acc. of 87.65%, sens. of 82.43%, and spec. of 89.67%. Also, the KNN manner has outperformed high performance with an acc. of 91%, sens. of 90%, and spec. of 83%. Besides, the ODNN method has showcased competitive outcomes with an acc. of 94.56%, sens. of 92.20%, and spec. of 94.20%. However, the presented DLMN-DBN technique has obtained effective diagnostic performance with an acc. of 95.55%, sens. of 93.94%, and spec. of 96.49%.

The Table 5 portrayed that the ANN model has accomplished inferior outcomes by achieving a lower PPV of 70% and NPV of 76%. In line with, the MLP model has achieved a slightly increased PPV of 72% and NPV of 79%. Besides, the DNN model has resulted in an even higher PPV of 72% and NPV of 80%. At the same time, the KNN model has showcased a moderate outcome with the PPV of 73% and NPV of 71%. Moreover, the ODNN model has tried to show reasonable performance with

Table 5. Result Analysis of Existing with Proposed DLMN-DBN Method with respect to Acc., Sens., Spec. PPV and NPV

Methods	Acc.	Sens.	Spec.	PPV	NPV
DLMN-DBN	95.55	93.94	96.49	93.94	96.49
ODNN	94.56	92.20	94.20	87.00	74.00
MLP	82.00	77.00	72.00	72.00	79.00
RBF	84.00	86.00	54.00	92.00	86.00
Linear	77.00	89.00	36.00	89.00	70.00
ANN	86.00	87.00	79.00	70.00	76.00
KNN	91.00	90.00	83.00	73.00	71.00
DNN	87.65	82.43	89.67	72.00	80.00

the PPV of 87% and NPV of 74%. Furthermore, the linear model has exhibited high performance with a PPV of 89% and NPV of 70%. Additionally, the RBF model has demonstrated competitive results with a PPV of 92% and NPV of 86%. But the proposed DLMN-DBN model has achieved effective diagnostic performance with the PPV of 93.94% and NPV of 96.46%.

4 Conclusion

This study has developed a novel lung cancer diagnosis model in IoT and cloud enabled environment using DLMN-DBN model. The main advantage of the proposed system is that it helps to identify the disease at an early stage and thereby significantly improves the chances of survival. In addition to that lung cancer diagnosis can be automated by using the potential of Deep Learning and Deep Belief networks, which allows us to assess more cases in less time and cost. In the proposed system, the IoT devices are employed for the data acquisition process for lung cancer diagnosis and are then transmitted to the cloud server for diagnostic process. Then, the GF based preprocessing technique is applied for noise removal. Afterward, the feature vectors are extracted using DLMN model and finally, classification process happens by the utilization of DBN model. A series of simulations were performed to ensure the effective result analysis of the DLMN-DBN model. The experimental values stated that the DLMN-DBN model has resulted in higher accuracy, sensitivity, and specificity of 95.55%, 93.94%, and 96.49% respectively than the existing systems. As a part of future scope, the performance of the DLMN-DBN model can be increased by the use of hyperparameter optimization techniques.

References

1) Mishra S, Thakkar HK, Mallick PK, Tiwari P, Alamri A. A sustainable IoHT based computationally intelligent healthcare monitoring system for lung cancer risk detection. *Sustainable Cities and Society*. 2021;72:103079. Available from: https://doi.org/10.1016/j.scs.2021.103079.
2) Valluru D, Jeya IJS. IoT with cloud based lung cancer diagnosis model using optimal support vector machine. *Health Care Management Science*. 2020;23(4):670–679. Available from: https://doi.org/10.1007/s10729-019-09489-x.
3) Revathi M, Jeya IJS, Deepa SN. Deep learning-based soft computing model for image classification application. *Soft Computing*. 2020;24(24):18411–18430. Available from: https://doi.org/10.1007/s00500-020-05048-7.
4) Sung H, Ferlay J, Siegel RL, Laversanne M, Soerjomataram I, Jemal A, et al. Global Cancer Statistics 2020: GLOBOCAN Estimates of Incidence and Mortality Worldwide for 36 Cancers in 185 Countries. *CA: A Cancer Journal for Clinicians*. 2021;71(3):209–249. Available from: https://doi.org/10.3322/caac.21660.
5) Mathur P, Sathishkumar K, Chaturvedi M, Das P, Sudarshan KL, Santhappan S, et al. Cancer Statistics, 2020: Report From National Cancer Registry Programme, India. *JCO Global Oncology*. 2020;6(6):1063–1075. Available from: https://doi.org/10.1200/GO.20.00122.
6) Bharathy S, Pavithra R, Akshaya B. Lung Cancer Detection using Machine Learning. In: Proceedings of the International Conference on Applied Artificial Intelligence and Computing (ICAAIC),2022. 2022.
7) Shakeel PM, Tolba A, Al-Makhadmeh Z, Jaber MM. Automatic detection of lung cancer from biomedical data set using discrete AdaBoost optimized ensemble learning generalized neural networks. *Neural Computing and Applications*. 2020;32(3):777–790. Available from: http://doi.org/10.1007/s00521-018-03972-2.
8) Toraman S, Girgin M, Üstündağ B, Türkoğlu İ. Classification of the likelihood of colon cancer with machine learning techniquesusing FTIR signals obtained from plasma. *Turk J Electr Eng Comput Sci*. 2019;27(3):1765–1779. Available from: http://doi.org/10.3906/elk-1801-259.
9) Krishna SL, Jeya IJS, Deepa SN. Fuzzy-twin proximal SVM kernel-based deep learning neural network model for hyperspectral image classification. *Neural Computing and Applications*. 2022;34(21):19343–19376. Available from: https://doi.org/10.1007/s00521-022-07517-6.
10) Suresh S, Mohan S. ROI-based feature learning for efficient true positive prediction using convolutional neural network for lung cancer diagnosis. *Neural Computing and Applications*. 2020;32(20):15989–16009. Available from: http://doi.org/10.1007/s00521-020-04787-w.
11) Masud M, Muhammad G, Hossain MS, Alhumyani H, Alshamrani SS, Cheikhrouhou O, et al. Light Deep Model for Pulmonary Nodule Detection from CT Scan Images for Mobile Devices. *Wireless Communications and Mobile Computing*. 2020;2020:1–8. Available from: http://doi.org/10.1155/2020/8893494.
12) Shakeel PM, Burhanuddin MA, Desa MI. Automatic lung cancer detection from CT image using improved deep neural network and ensemble classifier. *Neural Computing and Applications*. 2022;34(12):9579–9592. Available from: http://doi.org/10.1007/s00521-020-04842-6.

13) Kumar R, Singh DK, Mishra AK. An Approach to Extract Fine Detail and Unclear Information by Enhancing Computed Tomography Image. *2nd International Conference on Data, Engineering and Applications (IDEA)*. 2020. Available from: https://doi.org/10.1109/IDEA49133.2020.9170735.
14) Masud M, Sikder N, Nahid AA, Bairagi AK, Alzain MA. A Machine Learning Approach to Diagnosing Lung and Colon Cancer Using a Deep Learning-Based Classification Framework. *Sensors*. 2021;21(3):748. Available from: https://doi.org/10.3390/s21030748.
15) Venkatesh, Hegde SU. Fine-tuned MobileNet Classifier for Classification of Strawberry and Cherry Fruit Types. In: Proceedings of the International Conference on Computer Communication and Informatics (ICCCI). IEEE. 2021. Available from: https://doi.org/10.1109/ICCCI50826.2021.9402444.
16) Habib S, Alsanea M, Aloraini M, Al-Rawashdeh HS, Islam M, Khan S. An Efficient and Effective Deep Learning-Based Model for Real-Time Face Mask Detection. *Sensors*. 2602;22(7):2602. Available from: https://doi.org/10.3390/s22072602.
17) Yu J, Liu G. RETRACTED: Knowledge-based deep belief network for machining roughness prediction and knowledge discovery. *Computers in Industry*. 2020;121:103262. Available from: https://doi.org/10.1016/j.compind.2020.103262.
18) Nachimuthu DS, Jeya IJS, Baladhandapani AD. Adaptive extreme learning machine - Fuzzy system framework for energy optimization of IOTs in wireless sensor networks. *Internet Technology Letters*. 2021;(e267). Available from: https://doi.org/10.1002/itl2.267.